Supramolecular Chemistry

Ln(III) cyclen-based micelles and AuNPs conjugates as candidates for luminescent and magnetic resonance imaging (MRI) agents

Jennifer K. Molloy,*[1,2] Aline M. Nonat,*[2,3] John E. O'Brien,[2] Dermot F. Brougham[4] and Thorfinnur Gunnlaugsson*[2]

a.   Département de Chimie Moléculaire, UMR 5250, Université Grenoble Alpes, CNRS CS 40700, 38041, Grenoble cedex 9, France.

b.   School of Chemistry and Trinity Biomedical Sciences Institute, Trinity College Dublin, The University of Dublin, Dublin 2, Ireland. gunnlaug@tcd.ie

c.   SynPA, IPHC, UMR 7178, Université de Strasbourg, ECPM, 25 rue Becquerel, 67087 Strasbourg Cedex 02, France.

d.   School of Chemistry, University College Dublin, Belfield, Dublin 4, Ireland.

Corresponding Author:

Professor Thorfinnur Gunnlaugsson

School of Chemistry and Trinity Biomedical Sciences Institute

The University of Dublin, Trinity College Dublin

Dublin 2, Ireland

gunnlaut@tcd.ie

Telephone: +3531-896 3459

1
2
3
4
5
6
7
8
9
10
11
12
13
14
15
16
17
18
19
20
21
22
23
24
25
26
27
28
29
30
31
32
33
34
35
36
37
38
39
40
41
42
43
44
45
46
47
48
49
50
51
52
53
54
55
56
57
58
59
60

Ln(III) cyclen-based micelles and AuNPs conjugates as candidates for luminescent and magnetic resonance imaging (MRI) agents

Abstract

The luminescent lanthanide tetra-substituted cyclen (1,4,7,10-tetraazacyclododecane) based Eu(III), Tb(III),Gd(III) and Lu(III) complexes (1.Ln and 2.Ln) and the corresponding functionalised gold nanoparticles (1.Ln-AuNP) were developed for use in the formation of luminescent self-assembling ternary structures and as Gd-based MRI contrast agents. Nanoassemblies with spin-lattice relaxivities (r1) of 11.1 and 445 s-1mM-1 respectively (at 400 MHz) were obtained, rationalised by a micellar arrangement of the 1.Gd complex or by the conjugation to AuNPs.

 Keywords: supramolecular chemistry, lanthanides, cyclen complexes, luminescence, MRI contrast agents, gold nanoparticles.

1. Introduction

The formation of smart imaging agents for use in both biochemical and medical applications is a topical area of research.[1,2] In that area, the use of structures (such as fluorophores) that can self-assemble into higher order supramolecular assemblies,[3] or be used for surface functionalization,[4] is highly desirable.[5] In particular, dual modal contrast agents with optical imaging and magnetic resonance imaging (MRI) properties can combine the excellent anatomical and spatial resolution of MRI with the acute sensitivity of optical based imaging probes.[3,4,6] In the past we have developed several examples of targeting luminescent sensors, probes and MRI imaging agents.[7] Given their remarkable biocompatibility and versatile surface functionalization,[1,8] gold nanoparticles (**AuNPs**) have received significant interest for use in multiple imaging technologies.[1e,9]

We have shown that lanthanide based AuNPs can be used in pH and anion sensing, as well as in luminescent imaging of microcracks in bones, using Eu(III) tetra-substituted cyclen (1,4,7,10-tetraazacyclododecane) systems.[10] Cyclen-based[1f] Gd(III) complexes are also excellent candidates for developing MRI contrast agents and they are currently used in approximately 40% of all MRI examinations, *e.g.* about 40 million administrations of [Gd(DOTA)]$^-$ annually.[5b] Recent research has demonstrated that higher longitudinal relaxivities (^{1}H T$_1$ relaxation enhancements per mM agent) are, however, required to enable targeted and molecular imaging or to improve contrast-enhanced brain tumour MRI imaging. Systems such as particles can act as platforms to achieve that,[6] as this allows (*i*) an increase in the Gd(III) content (*via* the incorporation of several Gd(III) complexes on the same nano-object, aggreigates, *etc.*),[8] and; (*ii*) a reduction in the tumbling rate of the complexes. Examples of macromolecular hybrid systems that have recently been developed with this in mind,[2a] include: dendrimers, micelles and peptides,[9,11] carbon nanotubes[12] and nanoparticles.[13] In this communication we demonstrate that unsaturated tetra-substituted cyclen-based lanthanide complexes possessing a hydrophobic tail (with or without a terminal thiol) can be used in the construction of nano-based dual imaging probes capable of both luminescent sensing[14,15] and MRI contrast enhancement. We present two types of complexes based on a tri-acetamide derived cyclen ligand **1.Ln** and **2.Ln**, Figure 1; the former containing a terminal thiol group to facilitate functionalization of **AuNPs** and the second a dodecane chain, which we have recently shown can promote the formation of micelles[16]. We demonstrate that the Eu(III) complexes of **1** and **2** form luminescent ternary complexes with β-diketonates such as **nta** (4,4,4-trifluoro-1-(2-naphthyl)butane-1,3-dione) and **tta** (4,4,4-Trifluoro-1-(2-thienyl)-1,3-butanedione) and

that the Gd(III) complexes of these ligands give significant enhancement of the longitudinal ^{1}H relaxivity (MRI contrast efficiency).

2. Results and Discussion

2.1 Synthesis and characterisation studies

The synthesis of ligand **1** was carried out by monoalkylation of cyclen,[14,15] alkylation of the remaining six amines with bromoacetamide, followed by reductive cleavage of the disulfide bridge, which formed **1** in overall 20 % yield over the 3 steps (*c.f.* characterisation in SUPPORTING INFORMATION). The model compound **2**, which lacks the terminal thiol group, was formed using a similar synthetic strategy. This compound was chosen to act as a control as the thiol may partially displace one of the metal bound water molecules in H_2O and buffered solution, as we previously observed in the development of NIR based **Yb-AuNP** pH sensors.[10] The corresponding lanthanide complexes **x.Ln** where x= **1** and **2**, using Eu(III), Gd(III) and Tb(III), were then formed by complexation of **1** and **2** with 1.1 eqs. of the corresponding $Ln(CF_3SO_3)_3$ in yields ranging from 70-85 %, after precipitation and conventional workup (See ESI).

   The synthesis of **AuNP-1.Ln** (**Ln** = Eu(III), Tb(III), and Gd(III)) was achieved with modification[10a,14] of the two-phase Brust-Schiffrin method.[17] Phase transfer was achieved with **1.Ln** in H_2O to form **1.Ln-AuNPs**, which were characterized by measuring the UV-Vis absorption spectrum in H_2O. The characteristic plasmon (SPR) band of the **AuNPs** at 520 nm was indicative of the formation of gold nanoclusters of size in the 2- 10 nm range (*c.f.* SUPPORTING INFORMATION).

Moreover, this band was indicative of very good stability of the particles in water, as no measurable changes were detected over a period of six months.

Transmission electron microscopy (TEM) images of **1.Eu-AuNPs** also showed the formation of spherical monodisperse nanoparticles with an average diameter of 5 nm (standard deviation 0.3 nm, Figure 2 left) and no evidence of aggregation, which often can occur, as we have demonstrated in the formation of Ru(II)-polypyridyl based **AuNPs**,[7a,b] Figure 2. The size distribution was further confirmed using dynamic light scattering (DLS), which shows the formation of particles of approximate size 5 nm for **1.Eu-AuNPs,** Figure 2 right. These particles were found to be stable in aqueous media over period of many months. Having synthesised and characterised **1.Ln**, **2Ln** and **1.Ln-AuNPs**, we next set out to investigate their photophysical properties,[14,18-20] in aqueous media, in the absence and the presence of the antennae **nta** and **tta.**

2.2 Photophysical studies of Eu(III), Tb(III) complexes and Ln-AuNPs

The excited state lifetimes (τ) of the complexes, **1.Ln**, in both D_2O (τ = 0.93 ms for **1.Eu** and 1.6 ms for **1.Tb)** and H_2O (τ = 0.44 ms for **1.Eu** and 0.64 ms for **1.Tb)** were measured, which in both cases gave the hydration number, q (the number of metal bound water molecules) as 1.[18] The results are summarised in Table 1. These complexes are designed to be hepta coordinated,[19,20] and hence, once would expect q to be 2, to fulfil the high coordination number of both Eu(III) or Tb(III). However, for other thiol containing cyclen systems we have seen that the thiol functional group can coordinate to the ion reducing the overall hydration state,[10a-b,] so suggest that a similar effect is operating here. The lifetimes of

1.Eu-AuNPs and **1.Tb-AuNPs** were also determined; the same trend as the free complex was observed; with τ = 1.67 and 2.7 ms (in D_2O) and τ = 0.64 and 1.6 ms (in H_2O) for **1.Eu-AuNPs** and **1.Tb-AuNPs**, respectively. While conjugation to the **AuNP**s reduces all the lifetimes, the fact that the trends are retained demonstrates that conjugation to the particles does not significantly alter the coordination environment of the lanthanide ion, and q remains unchanged at ~1. In contrast, the model compound **2.Ln** (which lacks the terminal thiol) demonstrated lifetimes of τ = 1.14 ms for **2.Eu** in D_2O and τ = 0.52 ms for **2.Eu** in H_2O, consistent with the presence of two metal bound water molecules, as expected for such coordinatively unsaturated structures.

Metal-bound solvent molecules are known to quench the luminescence of lanthanides due to the presence of OH oscillators[18] and thus the utilization of these complexes in luminescent imaging requires the replacement of the metal bound water molecules to form ternary complexes. To investigate this, the "switching on" of the Eu(III) entered emission, and the concomitant formation of **1.Eu** and **1.Eu-nta** was monitored by luminescence titration using the **nta** antenna upon excitation at 330 nm, Figure 3 and 4, respectively. As as can be seen in Figure 3, the Eu(III) centred emission of **1.Eu-nta** was similarly "switched on", but at much higher equivalents than seen for **1.Eu** (see discussion below). The formation of the ternary complex between the antennae and the complexes was evident from the enhancement in the line-like emission bands at 580, 595, 616, 650, and 700 nm, assigned to the characteristic population of the $^5D_0$ excited state, which deactivated to the ^7F_J (J = 0, 1, 2, 3, and 4) ground state. Of these, the hypersensitive ΔJ = 2 transition, centred at 616 nm, is particularly

sensitive to the coordination environment of the Eu(III) centre, demonstrating direct coordination to the metal ion upon replacement of the water molecules, as was evident from lifetime measurements which resulted in determination of q as 0. Plotting the changes in the $\Delta J = 2$ transition as a function of **nta** equivalents showed an emission plateau after the addition of one equivalent (inset Figure 3) demonstrating 1:1 binding between the bidentate antenna, **nta**, and **1.Eu**. The titration of **1.Eu** with **tta** also demonstrated 1:1 binding; the emission being switched on in an identical manner to that for **nta**. The reference compound **2.Eu** demonstrated the same trend, and confirmed the 1:1 stoichiometry; showing that the complexes had similar coordination spheres to that seen for **1.Eu**.

As expected, due to the presence of two metal bound water molecules, the corresponding Tb(III) complexes were initially found to be non-luminescent in HEPES buffered solution (pH 7.4, NaCl 0.1 M ionic strength). However, as in the case of Eu(III), they gave rise to the formation of luminescent ternary adducts with 1:1 stoichiometry upon titration with suitable antennae (that can populate the $^{5}D_{4}$ excited state of Tb(III))[14,24] such as benzoic acid and terephthalic acid, chosen due to their triplet state levels (See SUPPORTING INFORMATION) for both **1.Tb** and **2.Tb**, confirming the results above for Eu(III).

Having established that both complexes could be employed for the formation of ternary complexes in competitive media, we carried out similar titration using **1.Eu-AuNPs** in the same media. The results are shown in Figure 4, demonstrating that upon stepwise formation of the ternary complexes on the **AuNPs** the emission was 'switched on' in a similar manner to that of **1.Eu** alone.

We have previously demonstrated that such progressive 'switching on' is highly depended on the number of complexes on the surface of the **AuNP**.[14,15a] The overall titration profile (from 0→250 equivalents of the antenna) is shown as inset in Figure 4, showing a 10-fold increase in the Eu(III) centred emission; this enhancement corresponding to the displacement of the hydration molecules of the surface-bound complexes. The concentration of **AuNPs** can be determined using the SPR of the particles; for which a plateau was observed upon addition of 50 equivalents of **nta**. Consequently, using the 1:1 stoichiometry determined above, it can be estimated that 50 **1.Eu** were present on the surface of the particle **AuNP** in **1.Eu-AuNPs**; which is in good agreement with our previous work using Ln-functionalised **AuNPs**.[14] This was further confirmed by carrying out such titrations using **1.Tb-AuNPs**; the Tb(III) emission also being switched on within a similar equivalents range of the antenna. As the **1.Eu-AuNP** conjugates were developed for potential applications such as luminescent sensing and imaging, the effect of pH on the luminescent properties of **1.Ln** and **1.Ln-AuNP** was evaluated for their stability and photophysical response over a broad pH range from 2-12. Gratifyingly, the change in pH results only in a small bathochromic shift in the antenna band at 339 nm with a concomitant hyperchromic shift (See SUPPORTING INFORMATION) whereas the band at 265 nm band experienced a hypochromic shift. The pH-luminescent profile also demonstrated (See SUPPORTING INFORMATION) that **1.Eu-AuNPs-nta** was most luminescent construct at physiological pH; making it a particularly attractive nano-system for bio-applications. Having confirmed the presence of metal ion bound water molecules in **1.Eu** and **1.Eu-AuNPs** over a wide pH range,

the isostructural gadolinium complexes **1.Gd** and **1.LGd-AuNPs** were prepared and investigated as potential nanostructured MRI contrast agents.

2.3 Relaxivity measurements of Gd(II) complexes and AuNP conjugate

The efficiency of Gd(III) complexes in aqueous media for enhancing contrast in T_1-weighted MRI is quantified by the ^{1}H relaxivity $r_1 = [(1/T_1) - (1/T_1)_{Gd=0}] / [Gd]$. The results of the relaxivity measurements for **1.Gd** are shown in Figure 5, and demonstrate an r_1 value of 11.1 $s^{-1}mM^{-1}$ at 400 MHz, which is surprisingly high in comparison to previously reported mono-aquo Gd(III) of similar molecular weight.[21] This suggests organization of this complex into more complex architectures in solution; very likely due to the formation of assemblies such as micelles which alter the dynamics about the metal ion. In order to assess the rotational dynamics of the complex **1.Gd** at this concentration (C_{Gd} =2.67 mM), it became thus apparent that it was important to estimate its hydrodynamic radius (r_H) under these conditions. This value can be obtained by measuring the translational diffusion coefficient by PFG–NMR with application of the Stokes-Einstein Model.[22] The diffusion coefficients of **1.Eu** and **1.Lu** (D = 2.89) were thus determined in D_2O at 298 K, from which a r_H value of 60 Å was determined for both complexes. This value is much larger than expected for complexes of this size; suggesting the formation of aggregates/micelles, which was further confirmed by DLS measurements which, despite the inevitable strong size dependent weighting, also showed the presence of aggregates with r_H between 50-100 Å. Luminescence lifetime measurements, performed on **1.Eu** at the same concentration (τ_{H2O} = 0.44 ms and τ_{D2O} = 0.93 ms), indicated that the

coordination sphere of the Eu(III) was unchanged upon micelle formation, and the Ln(III) complexes remained as heptacoordinate (*e.g.* q = 1). An approximate value of the critical micelle concentration was also determined by NMR PFG-NMR and DLS to be 0.15×10^{-3} M. Hence, the results indicate that the organization of **1.Gd** into micellar structures with slow tumbling rates, together with fast water-exchange rate of the one metal-bound water molecule, are the likely cause of the unusually high relaxivities measured at C_{Gd} = 2.67 mM.

NMR and DLS studies were also undertaken for both **2.Eu** and **2.Lu** within the same concentration range of 0.1 → 10 mM. These results (See SUPPORTING INFORMATION) indicated the absence of any aggregates for **2.Eu** and **2.Lu**; suggesting that, as expected, the thiol terminal group is key to the formation of aggregates for **1.Ln**. This finding was also confirmed by the relaxivity studies for **2.Gd**; with a significantly lower relaxivity value of r_1 = 5.80 $s^{-1}mM^{-1}$ at 400 MHz as compared to **1.Gd**, which is more typical of that anticipated for bis-aquo complexes of this size. For instance, r_1 values ranging from 5.6 to 10.5 $s^{-1}mM^{-1}$, at 25 °C and 20 MHz, have previously been measured, under similar conditions, for the HOPO-based Gd(III) complexes [Gd(DO3A)(H$_2$O)$_2$].[23] We suggest that the role of thiol group in supramolecular structure formation is to promote the formation of a hydrophobic pocket with the charged Ln(III) complexes acting as a hydrophilic head. Hence, these results suggest thiol-functionalised derivatives as particularly attractive targets for the design of new high relaxivity micellar structures.

The conjugation of the complexes onto **AuNPs** to form **1.Gd-AuNPs** might be expected to further increase the relaxivity by reducing the tumbling rates, in any

case high lanthanide loading per particle (*c.*50 Gd(III) ions per **AuNP**) is also advantageous. The longitudinal [1]H r_1 value of **1.Gd-AuNP** was found to be 4.42 s^{-1}mM^{-1}, at 2.67 mM (Gd) and 400 MHz. The relaxivity per **AuNP** was found to be significantly larger than was observed for the **1.Gd** micellar systems, probably due to the very high Gd content on the AuNPs. Analysis of the relaxivity of **1.Gd-AuNP** as a function of temperature, demonstrated a decrease in r_1 with increasing temperature. This suggests that the water exchange rate at room temperature is not a limiting factor for the relaxivity. Nevertheless the measured NMRD profile is not indicative of slow rotation with fast water exchange rate. Moreover, a lower relaxivity of 4.42 mM^{-1}s^{-1} per Gd(III) ion compared to the value for free **2.Gd** of 5.8 mM^{-1}s^{-1} at 400 MHz, suggests that at the attainable grafting density any restriction to internal dynamics conferred by particle grafting had little effect on the relaxivity. This is potentially due to internal rotation due to the flexible alkyl chain.

3. Conclusion

Herein, we have developed and investigated a series Ln-complex of **1**; **1.Eu**, **1.Gd** and **2.Eu** and **2.Gd** and the conjugated **1.Ln-AuNPs** nano-structures. Our results demonstrate that each **1.Ln** complex contained a single metal bound water molecule; both in the free complexes and upon surface conjugation to **AuNPs.** In contrast, **2.Ln**, which lacks the terminal thiol group in **1.Ln**, were formed with *q* =2. The photophysical properties of the **1.Eu** and **1.Tb** analogues were also studied; and the presence of one inner sphere water molecule, and the formation of luminescent ternary complexes with the **nta** and **tta** antennae, was

confirmed. We also shown that the **1.Gd** complex has a relatively high relaxivity of 11.5 mM^{-1}s^{-1} compared to other similar mono-aquo cyclen complexes, which we attribute to the formation of aggregates, or micellar formation in solution; with a CMC of 0.15×10^{-3} M. **1.Ln-AuNPs** nanostructures were also characterized, and shown to possess a high relaxivity due to high loading of (*ca*. 50) **1.Gd** complexes per **AuNP**. However, the relaxivity per Gd ion remains limited by a fast τ_R, probably due to flexible chains allowing free rotation. To conclude, the work herein supports our endeavour to develop novel and potential bimodal supramolecular nano-agents possessing both luminescent and magnetic Ln(III) properties. Future work will be directed towards the formation of functional bimodal systems for the development of more targeted/responsive contrast agents.

4. Experimental

2,2',2''-(10-(12-Mercaptododecyl)-1,4,7,10-tetraazacyclododecane-1,4,7-triyl)triacetamide

Mercaptododecanyl tetraazacyclododecane (0.123 g, 0.332 mmoles, 1eq.) was dissolved in CH$_3$CN with K$_2$CO$_3$ (0.151 g, 1.1 mmoles, 3.3 eq.) and KI (0.176 g, 1.1 mmoles, 3.3 eq.). Bromoacetamide (0.15 g, 1.1 mmoles, 3.3 eq.) was added to the solution and the solution stirred for 5 days at 85 °C. Reductive cleavage with NaBH$_4$ (2eq.), followed by washing with water, dried over MgSO$_4$, filtered and solvent removed followed by two precipitations in ether and methanol yielded the product as a yellow clear oil 0.090 g, 51% yield. HRMS (*m/z*-ES+) Found for C$_{26}$H$_{54}$N$_7$O$_3$S: 544.4026, Required 544.4009; δ_H (MeOD, 400 MHz): 3.26 (CH$_2$), 3.18 (CH$_2$), 3.02 (CH$_2$), 1.70 (CH$_2$),

1.51 (CH$_2$), 1.30 (CH$_2$ chain). δ$_C$ (MeOD, 100 MHz): 175.7(q), 175.1(q), 169.3(q), 56.8 (Cyclen CH$_2$), 56.5 (Cyclen CH$_2$), 54.6 (Cyclen CH$_2$), 54.4 (CH$_2$), 51.3(CH$_2$), 51.2 (CH$_2$), 50.7 (CH$_2$), 50.1 (CH$_2$), 38.8 (CH$_2$), 29.8 (CH$_2$), 29.7 (CH$_2$), 29.6 (CH$_2$), 29.64 (CH$_2$), 29.58 (CH$_2$), 29.3 (CH$_2$), 29.2 (CH$_2$), 29.1 (CH$_2$), 28.4 (CH$_2$), 28.3 (CH$_2$), 27.9 (CH$_2$), 27.8 (CH$_2$), 25.2 (CH$_2$), 7.1 (CH$_2$). v_{max} (neat sample)/ cm^{-1}: 3361, 3314, 3170, 2924, 2853, 2820, 1697, 1680, 1446, 1371, 1332, 1284, 1256, 1102, 1008, 907, 811, 722, 675.

General Procedure for the synthesis of 1.Ln

Ligand **1** was dissolved in MeOH with 1.1 eq. of Ln (CF$_3$SO$_3$)$_3$ and refluxed overnight under argon. Solvent was removed under reduced pressure and the resulting residue was precipitated out of swirling diethyl ether to yield 1.Ln as yellow oils.

1.Gd was isolated as a yellow oil, 0.0398 g, 47 % yield. HRMS (MALDI): Found 1186.14 for [**43.Gd** + (CF$_3$SO$_3$)$_3$ + K$^+$] Calculated: 1186.6786. v_{max} (neat sample)/ cm^{-1}: 3350, 3334, 2924, 2853, 1659, 1621, 1457, 1367, 1272, 1246, 1166, 1085, 1029, 915, 878, 834, 766, 720, 650.

1.Eu

1 (0.016 g, 0.0294 mmoles, 1eq.) was refluxed in MeOH with Eu(CF$_3$SO$_3$)$_3$ (0.019g, 0.0324 mmoles, 1.1eq.) to yield 0.0157 g, 77 % yield. δ$_H$ (MeOD, 400 MHz): -17.4, -15.35, -13.89, -11.6, -10.3, -8.7, -8.09, -7.8, -6.9, -5.5, -4.90, -3.05, -1.35, 0.29, 0.90, 1.34, 1.69, 2.02, 2.16, 2.70, 3.01, 3.14, 3.32, 3.35, 3.49, 3.63, 3.64, 3.69, 3.75, 4.05, 4.94, 5.5, 6.4, 8.1, 9.83, 13.53, 17.32, 18.45. v_{max} (neat sample)/ cm^{-1}: 3353, 3187, 2928, 2856, 1660, 1597, 1466, 1248, 170, 1083, 1028, 918, 832.

1.Lu

1 (0.028 g, 0.05 mmoles, 1 eq.) was dissolved in CH_3CN (10 mL) and the solution stirred with slow addition of $Lu(CF_3SO_3)_3$ (0.035 g, 0.056 mmoles, 1.1 eq.) to the solution followed by heating at reflux overnight. The solvent was reduced to 1 mL and the product precipitated out of ether to yield the product as a yellow oil 0.033 g, 92 % yield. δ_H (MeOD, 400 MHz): 3.86, 3.68, 3.48, 3.32, 3.19, 3.04, 2.99, 2.90, 2.83, 2.68, 2.20, 1.98, 1.69, 1.41, 1.30, 1.14; ν_{max} (neat sample)/ cm^{-1}: 3385, 3322, 3255, 2929, 2859, 1672, 1603, 1469, 1226, 1171, 1081, 1028, 917, 884, 837, 764.

1.Tb

43 (0.029g, 0.0537 mmoles, 1eq.) was dissolved in CH_3CN (20 mL) and stirred under reflux overnight with $Tb(CF_3SO_3)_3$ (0.0358 g, 0.059 mmoles, 1.1eq.) followed by precipitation from swirling diethyl ether to yield the product as a yellow oil 0.0353g, 93.5 % yield. δ_H (MeOD, 400 MHz): -155.1, -141.7, -116.1, -85.34, -55.9, -24.15, -15.0, -14.4, -13.7, -10.28, -9.6, -5.40, -2.77, -2.73, -1.46, -0.47, 0.04, 0.19, 0.49, 0.99, 1.19, 1.38, 1.49, 2.09, 2.31, 2.49, 3.33, 3.78, 4.85, 7.01, 15.52 302.6, 304.6, 306.0. ν_{max} (neat sample)/ cm^{-1}: 3348, 3174, 2927, 2855, 1657, 1596, 1463, 1249, 1173, 1081, 1029, 919, 833.

2,2',2''-(10-Dodecyl-1,4,7,10-tetraazacyclododecane-1,4,7-triyl)triacetamide

Dodecanyl tetraazacyclododecane (0.336 g, 0.98 mmoles, 1eq.) was dissolved in $CHCl_3$ with K_2CO_3 (0.45 g, 3.3 mmoles, 3.3 eq.) and KI (0.541 g, 3.3 mmoles, 3.3 eq.) and stirred with addition of bromoacetamide (3.3 eq.) at 0 ºC. The mixture was stirred for 7

14

days at 65 ºC before filtration through a plug of celite and removal of solvent. Extraction into $CHCl_3$ followed by washing with base, dried over $MgSO_4$, filtered and solvent removed under reduced pressure, yielded a white solid 0.0751 g, 15 % yield. HRMS (m/z-MALDI) Found for $C_{27}H_{55}N_3O_3$: 534.4103, Required: 534.4108; δ_H (MeOD, 400 MHz): 8.39 (1H, s, NH_2), 8.02 (2H, s, NH_2), 7.11 (1H, s, NH_2), 6.17 (1H, s, NH_2), 5.96 (2H, s, NH_2), 5.48 (2H, s, NH_2), 3.06 (6H, m, CH_2) 2.34 - 2.69 (16H, m, Cyclen), 1.28 (22H, m, CH_2), 0.89 (3H, m, CH_3). δ_C (MeOD, 100 MHz): 77.5 (CH_2). 77.2 (CH_2), 77.2 (CH_2), 77.1 (CH_2), 50.3 (CH_2), 50.0 (CH_2), 49.8 (CH_2), 49.6 (CH_2), 49.4 (CH_2), 49.3 (CH_2), 49.0 (CH_2), 31.9 (CH_2), 29.6 (CH_2), 29.5 (CH_2), 22.6 (CH_2), 14.1 (CH_2). ν_{max} (neat sample)/ cm^{-1}: 3356, 3257, 3167, 2919 (sharp), 2849, 1673, 1449, 1404, 1360, 1348, 1294, 1261, 1202, 1152, 1116, 1087, 1068, 1046, 1032, 1002, 979, 959, 923, 880, 803, 718, 669.

General procedure for synthesis of 2.Ln

2 was dissolved in MeOH and $Ln(CF_3SO_3)_3$ added to the mixture slowly. The solution was then refluxed overnight followed by reduction of the solvent to 1 mL under reduced pressure and precipitation out of swirling diethyl ether, which yielded the product as a yellow oil.

2.Eu

 2 (0.0144 g, 0.028 mmoles, 1 eq.) and $Eu(CF_3SO_3)_3$ (0.0185 g, 0.031 mmoles, 1.1 eq.) 0.0097 g, 52 % yield. HRMS (m/z-MALDI) Found for $C_{27}H_{52}N_7O_6F_3SEu$, 812.2834, Required: 812.2864; δ_H (MeOD, 400 MHz): 23.90, 21.56, 19.87, 19.09, 8.15, 7.92, 4.92, 3.69, 3.66, 3.49, 3.32, 3.05, 2.78, 2.66, 2.54, 2.05, 1.30, 0.92, 0.10, -.47, -1.19, -1.42, -1.70, -2.30, -2.60, -5.04, -5.44, -6.36, -7.95, -8.44, -9.17, -9.67, -11.24, -11.49, -12.01, -

1
2
3
4
5
6
7
8
9
10
11
12
13
14
15
16
17
18
19
20
21
22
23
24
25
26
27
28
29
30
31
32
33
34
35
36
37
38
39
40
41
42
43
44
45
46
47
48
49
50
51
52
53
54
55
56
57
58
59
60

13.79, -16.97, -18.01, -18.66; v_{max} (neat sample)/ cm^{-1}: 3357, 2926, 2856, 1666, 1600, 1467, 1235, 1217, 1165, 1082, 1025, 914, 880, 831, 762.

2.Gd

2 (0.0642 g, 0.125 mmoles, 1eq.) with Gd(CF$_3$SO$_3$) (0.0462 g, 0.138 mmoles, 1.1 eq.) yielded a white oily solid, 0.398 g, 47 % yield. HRMS (*m/z*-ES+) Found for C$_{27}$H$_{52}$N$_7$O$_6$F$_3$SGd 669.3474, Required: 669.3451. v_{max} (neat sample)/ cm^{-1}: 3367, 2930, 2856, 1603, 1467, 1237, 1217, 1164, 1079, 1025, 917, 880, 829, 764.

AuNPs

General Procedure: Tetrachloroaurate trihydrate was dissolved in Millipore water and stirred vigorously on addition of toluene containing tetraoctylammonium bromide (TOAB). The mixture was stirred vigorously at room temperature for 10 mins followed by addition of NaBH$_4$ slowly. The mixture was then stirred at room temperature for 2 hours. On cessation of stirring the product separated into the toluene layer as a dark purple solution. The product was extracted into toluene, washed with 0.1 M HCl, and 0.1 M NaOH followed by washing with H$_2$O. UV-vis absorption spectrum showed the characteristic SPR band of the **AuNPs** at 530 nm.

Eux.AuNP –General Synthesis

A 1 x 10^{-3} solution of complex in MeOH/H$_2$O was stirred vigorously on addition of toluene solution of nanoparticulate gold. The resulting water layer upon transfer of the gold to the complex solution turned deep purple showing stabilisation by the complex of the nanoparticle in the aqueous layer. The layers were then separated and

the aqueous layer filtered through a 0.2 μm pore syringe filter in order to remove possible aggregates. The resulting pink / purple solution (colour dependent on concentration of gold) contained the stabilized nanoparticles and the SPR in the UV-vis absorption spectrum could be seen to shift to approximately 520 nm.

Relaxometric measurements

The frequency dependence of the ^{1}H relaxation for the aqueous suspensions was recorded over the frequency range of 0.01 – 40 MHz using a Singmaster FFC-2000 Fast Field Cycling NMR Relaxometer (Stelar SRL, Mede, Italy). The system operated at a measurement frequency of 16.3 MHz for ^{1}H, at which frequency the 90° pulse was 7 $\Box$s. T_1 measurements were performed as a function of external field, B_0, with standard pulse sequences incorporating B_0 field excursions. For higher frequency measurements (40 – 80 MHz) a re-conditioned Bruker WP80 electromagnet was used. The temperature of the samples was maintained at 25 ±1 ^{o}C using a thermostatted airflow system. All of the ^{1}H magnetisation recovery curves were singly exponential within experimental error and the random errors in fitting T_1 were always less than 1%.

5. Supplementary Material

NMR, UV-Vis absorption and Emission studies, TEM and DLS results and NMRD results.

1
2
3
4
5
6
7
8
9
10
11
12
13
14
15
16
17
18
19
20
21
22
23
24
25
26
27
28
29
30
31
32
33
34
35
36
37
38
39
40
41
42
43
44
45
46
47
48
49
50
51
52
53
54
55
56
57
58
59
60

7. References

1. (a) Wahsner, J.; Gale, E. M.; Rodríguez-Rodríguez, A.; Caravan, P.; *Chem. Rev.*, **2019**, *119*, 957–1057; (b) Caravan, P.; Ellison, J. J.; McMurry, T. J.; Lauffer, R. B.; *Chem. Rev.* **1999**, *99*, 2293–2352; (c) Poynton, F. E.; Bright, S. A.; Blasco, S.; Williams, D. C.; Kelly J. M.; Gunnlaugsson, T.; *Chem. Soc. Rev.*, **2017**, *46*, 7706-7756; (d) Wu, D.; Sedgwick, A. C.; Gunnlaugsson, T.; Akkaya, E. U.; Yoon J.; James, T. D.; *Chem. Soc. Rev.*, **2017**, *46*, 7105-7123; (e) Surender, S., E. M.; Kotova, O.; Truman, L. K.; Molloy J. K.; Gunnlaugsson, T.; *Inorg Chem.*, **2014**, *53*, 1867-1879; (f) Heffern, M. C.; Matosziuk L. M.; Meade, T. J.; *Chem. Rev.*, **2014**, *114*, 4496. (g) Gunnlaugsson T.; Parker, D.; *Chem. Commun.*, **1998**, 511–512; (h) Nonat, A. M.; Harte, A. J.; Senechal-David, K.; Leonard J. P.; Gunnlaugsson, T.; *Dalton Trans.*, **2009**, 4703–4711.

2. (a) Caravan, P. *Chem. Soc. Rev.* **2006,** *35,* 512-523. (b) Alric, C.; Taleb, J.; Le Duc, G.; Mandon, C.; Billotey, C.; Le Meur-Herland, A.; Brochard, T.; Vocanson, F.; Janier, M.; Perriat, P.; Roux S.; Tillement, O.; *J. Am. Chem. Soc.* **2008,** *130,* 5908-5915.; (c) Greish, K.; *J. Drug Target.* **2007,** *15*, 457-464. (d) Kunjachan, S.; Ehling, J.; Storm, G.; Kiessling, F.; Lammers, T.; *Chem. Rev.*, **2015**, *115,* 10907; (e) Amoroso, A. J.; Pope, S. J. A.; *Chem. Soc. Rev.*, **2015**, *44*, 4723. (f) Meledandri, C. J.; Brougham, D. F.; *Anal. Method*s, **2012**, *4*, 331; (g) Gun'ko, Y. K.; Brougham, D. F.; *Nanotechnologies for the Life Sciences*, Wiley-VCH, **2009**, *4*, 119–185.

3. (a) Savyasachi, A. J.; Kotova, O.; Shanmugaraju, S.; Bradberry, S. J.; Ó Máille, G. M.; Gunnlaugsson, T.; *Chem*, **2017**, *3*, 764–811. (b) Tallec, G.; Imbert, D.; Fries P. H.; Mazzanti, M.; *Dalton Trans.* **2010**, *39,* 9490-9492.

4. (a) Lacerda S.; Tóth, É.; *Chem. Med. Chem.* **2017,** *12*, 883-894; (b) Li, X.-Z.; Zhou, L.-P.; Yan, L.-L.; Yuan, D.-Q.; Lin C.-S.; Sun, Q.-F.; *J. of the Am. Chem. Soc.* **2017,** *139,*

8237-8244; (c) Goetz, J.; Nonat, A.; Diallo, A.; Sy, M.; Sera, I.; Lecointre, A.; Lefevre, C.; Chan, C.F.; Wong, K.-L.; Charbonnière, L. J.; *Chem. Plus. Chem.* **2016**, *81*, 526-534.

5. (a) Lohrke, J.; Frenzel, T.; Endrikat, J.; Alves, F. C.; Grist, T. M.; Law, T. M.; Lee, J. M.; Leiner, T.; Li, K. C.; Nikolaou, K.; Prince, M. R.; Schild, H. H.; Weinreb, J. C.; Yoshikawa K.; Pietsch, H.; *Adv. Ther.* **2016**, *33*, 1-28; (b) Hao, D.; Ai, T.; Goerner, F.; Hu, X.; Runge V. M.; Tweedle, M.; *J. Magn. Res. Imag.* **2012**, *36,* 1060-1071.

6. (a) Meola, A.; Rao, J.; Chaudhary, N.; Sharma M.; Chang, S. D.; *Gold Front. Neurol.* **2018**, *9,* 328. (b) Nicolay, K.; Strijkers G.; Grüll, H.; *The Chemistry of Contrast Agents in Medicinal Magnetic Resonance Imaging*, John Wiley & Sons, Ltd, **2013**, *11*.

7. (a) Martínez-Calvo, M.; Orange, K. N.; Elmes, R. B. P.; la Cour Poulsen, B.; Williams D. C.; Gunnlaugsson, T.; *Nanoscale*, **2016**, *8,* 563-574; (b) Elmes, R. B. P.; Orange, K. N.; Cloonan, S. M.; Williams D. C.; Gunnlaugsson, T.; *J. Am. Chem. Soc.,* **2011**, *133*, 15862-15865. (c) McMahon, B. K.; Mauer, P.; McCoy, C. P.; Lee T. C.; Gunnlaugsson, T.; *J. Am. Chem. Soc.*, **2009**, *131*, 17542. (d) Surender, E. M.; Bradberry, S. J.; Bright, S. A.; McCoy, C. P.; Williams D. C.; Gunnlaugsson, T.; *J. Am. Chem. Soc.*, **2017**, *139*, 381-388.

8. (a) Langereis, S.; Dirksen, A.; Hackeng, T. M.; van Genderen M. H. P.; Meijer, E. W.; *New J. Chem.* **2007**, *31*, 1152-1160. (b) Aime, S.; Castelli, D. D.; Crich, S. G.; Gianolio, E.; Terreno, E.; *Acc. Chem. Res.* **2009,** *42,* 822-831. (c) Lacerda, S.; Bonnet, C. S.; Pallier, A.; Villette, S.; Foucher, F.; Westall, F.; Buron, F.; Suzenet, F.; Pichon, C.; Petoud S.; Tóth, E.; *Small*, **2013**, *9,* 2662; (d) Debroye, E.; Laurent, S.; Elst, L. V.; Muller R. N.; Parac-Vogt, T. N.; *Chem. Eur. J.*, **2013**, *19,* 16019. (e) Poznik, M.; Maitrab U.; Konig, B.; *Org. Biomol. Chem.*, **2015**, *13*, 9789; (f) Iqbal, U.; Albaghdadi, H.; Nieh, M.; Tuor, U. I.; Mester, Z.; Stanimirovic, D.; Katsaras J.; Abulrob, A.; *Nanotechnolog*y, **2011**, *22*, 195102; (g) Terreno, E.; Boffa, C.; Menchise, V.; Fedeli, F.; Carrera, C.; Castelli, D. D.;

1
2
3
4
5
6
7
8
9
10
11
12
13
14
15
16
17
18
19
20
21
22
23
24
25
26
27
28
29
30
31
32
33
34
35
36
37
38
39
40
41
42
43
44
45
46
47
48
49
50
51
52
53
54
55
56
57
58
59
60

Digiliod G.; Aime, S.; *Chem. Commun*., **2011**, *47*, 4667; (e) Kozlowska, D.; Biswas, S.; Fox, E. K.; Wu, B.; Bolster, F.; Edupuganti, O. P.; Torchilin, V.; Eustace, S.; Botta, M.; O'Kennedy, R.; Brougham, D. F.; *RSC Adv*., **2014**, *4*, 18007.

9. (a) Lewis D. J.; Pikramenou, Z.; *Coord. Chem. Rev*., **2014**, *273*, 213; (b) Cheng, Z.; Thorek, D. L. J.; Tsourkas, A.; *Angew. Chem. Int. ed.,* **2010,** *49*, 346-350. c) Bonnet, C. S.; Pellegatti, L.; Buron, F.; Shade, C. M.; Villette, S.; Kubicek, V.; Guillaumet, G.; Suzenet, F.; Petoud S.; Tóth, É.; *Chem. Commun*., **2010**, *46,* 124;

10. (a) Surender, E. M.; Comby, S.; Cavanagh, B.; Brennan, O.; Lee T. C.; Gunnlaugsson, T.; *Chem*, **2016**, *1*, 438–455. (b) Truman, L. K.; Comby S.; Gunnlaugsson, T.; *Angew. Chem. Int. Ed.,* **2012**, *51*, 9624-9627; (b) Comby S.; Gunnlaugsson, T.; *ACS Nano*., **2011,** *5*, 7184–7197.

11. (a) Park, J.- A. ; Lee, J.-J.; Jung, J.-C.; Yu, D.-Y.; Oh, C.; Ha, S.; Kim, T.-J.; Chang, Y. *Chem. Bio. Chem.* **2008**, *9***,** 2811-2813. (b) Nicolle, G. M.; Tóth, É.; Eisenwiener, K.-P.; Mäcke, H. R.; Merbach, A. E. *; J. Biol. Inorg. Chem.* **2002**, *7*, 757-769; (c) Torres, S.; Martins, J. A.; André, J. P.; Geraldes, C. F. G. C.; Merbach, A. E.; Tóth, É.; *Chem. Eur. J.* **2006**, *12***,** 940-948.

12. Chen, K.; Chen, X.; *Curr. Top. Med. Chem.* **2010**, *10,* 1227-1236.

13. (a) Park, J.-A.; Reddy, P. A. N.; Kim, H.- K.; Kim, I.-S.; Kim, G.-C.; Chang, Y.; Kim, T.-J.; *Bioorg. Med. Chem. Lett.* **2008**, *18*, 6135-6137; (b) Pansieri, J.; Plissonneau, M.; Stransky-Heilkron, N.; Dumoulin, M.; Heinrich-Balard, L.; Rivory, P.; Morfin, J.-F.; Tóth, É.; Saraiva, M. J.; Allémann, E.; Tillement, O.; Forge, V.; Lux, F.; Marquette, C.; *Nanomedicine* **2017**, *12*, 1675-1687. (c) Moriggi, L.; Cannizzo, C.; Dumas, E.; Mayer, C. R.; Ulianov, A.; Helm, L.; *J. Am. Chem. Soc.* **2009**, *131*, 10828-10829.

14. Truman, L. K.; Bradberry, S. J.; Comby, S.; Kotova, O.; Gunnlaugsson, T.; *ChemPhysChem*, **2017**, *18*, 1746-1751.

15. (a) Massue, J.; Quinn, S. J.; Gunnlaugsson, T.; *J. Am. Chem. Soc.* **2008**, *130*, 6900-6901; (b) Bonnet, C. S.; Massue, J.; Quinn, S. J.; Gunnlaugsson, T.; *Org. Biomol. Chem.* **2009**, *7*, 3074-3078.

16. Surender, E. M.; Comby, S.; Martyn, S.; Cavanagh, B.; Lee, T. C.; Brougham, D. F.; Gunnlaugsson, T.; *Chem. Commun*. **2016**, *52*, 10858-10861.

17. (a) Brust, M.; Walker, M.; Bethell, D. ; Schiffrin, D. J.; Whyman, R.; *J. Chem. Soc., Chem. Commun.* **1994**, 801-802. (b) Li, Y.; Zaluzhna, O.; Xu, B.; Gao, Y.; Modest, J. M.; Tong, Y. J.; *J. Am. Chem. Soc.* **2011**, *133*, 2092-2095.

18. (a) Supkowski, R. M.; Horrocks, W. D.; *Inorg. Chim. Acta,* **2002**, *340***,** 44-48. (b) Beeby, A.; Clarkson, I. M.; Dickins, R. S.; Faulkner, S.; Parker, D.; Royle, L.; de Sousa, A. S.; Williams, J. A. G.; Wood, M.; *J. Chem. Soc., Perkin Trans. 2,* **1999**, 493-504.

19. Butler, S. J.; Parker, D.; *Chem. Soc. Rev.* **2013**, *42*, 1652-1666.

20. (a) Pope, S. J. A.; Burton-Pye, B. P.; Berridge, R.; Khan, T.; Skabara, P. J.; Faulkner, S. *Dalton Trans.* **2006**, 2907-2912. (b) Gunnlaugsson, T.; Harte, A. J.; Leonard, J. H. P.; Nieuwenhuyzen, M.; *Supramol. Chem.* **2003**, *15*, 505-519.

21. Powell, D. H.; Ni Dhubhghaill., O. M.; Pubanz, D.; Helm, L.; Lebedev, Y. S.; Schlaepfer, W.; Merbach, A. E.; *J. Am. Chem. Soc.* **1996**, *118*, 9333-9346.

22. Lycknert, K.; Rundlöf, T.; Widmalm, G.; *J. Phys. Chem. B.* **2002**, *106***,** 5275-5280.

23. Datta, A.; Raymond, K. N.; *Acc. Chem. Res.* **2009**, *42*, 938-947.

1
2
3
4
5
6
7
8
9
10
11
12
13
14
15
16
17
18
19
20
21
22
23
24
25
26
27
28
29
30
31
32
33
34
35
36
37
38
39
40
41
42
43
44
45
46
47
48
49
50
51
52
53
54
55
56
57
58
59
60

Figure Captions

Figure 1 Figure 1. The Ln(III) cyclen complexes and antennae structures used in this study.

Figure 2. Left: TEM image of **1.Eu-AuNPs**, with size distribution inset (each bar representing 1-8 nm). Right: Dynamic Light Scattering (DLS) of **1.Eu-AuNPs** in H_2O from two different samples**.**

Figure 3: Figure 2: Changes in the Eu(III) emission of **1.Eu** (c =1 x 10-5 M) in HEPES buffered solution (0.1 M, ionic strength 0.1M HCl) upon addition of **nta** (0-6 equivalents) *Inset:* The changes in the Δ *J* = 2 transition versus the number of equivalents of **nta** added.

Figure 4: The changes in the Eu(III) emission of **1.Eu-AuNPs** (50 complexes per particle) (1×10^{-7}M of **AuNPs**) in HEPES buffer at pH 7.4 (0.1M, ionic strength 0.1M NaCl) upon the addition of **nta** from 0-250 equivalents. *Inset:* The changes in the Δ *J* = 2 transition versus the number of equivalents of **nta** added.

Figure 5: Longitudinal relaxivity (r_1) of the protons of H_2O with **1.Gd** (Red squares) (2.67 mM) and **1.Gd-AuNP** (black squares), (2.7 mM) squares represent the r_1 per **AuNP**.

1
2
3
4
5
6
7
8
9
10
11
12
13
14
15
16
17
18
19
20
21
22
23
24
25
26
27
28
29
30
31
32
33
34
35
36
37
38
39
40
41
42
43
44
45
46
47
48
49
50
51
52
53
54
55
56
57
58
59
60

Figures

Figure 1:

1.Ln

nta

2. Ln

tta

Figure 2

Size distribution by volume

1
2
3
4
5
6
7
8
9
10
11
12
13
14
15
16
17
18
19
20
21
22
23
24
25
26
27
28
29
30
31
32
33
34
35
36
37
38
39
40
41
42
43
44
45
46
47
48
49
50
51
52
53
54
55
56
57
58
59
60
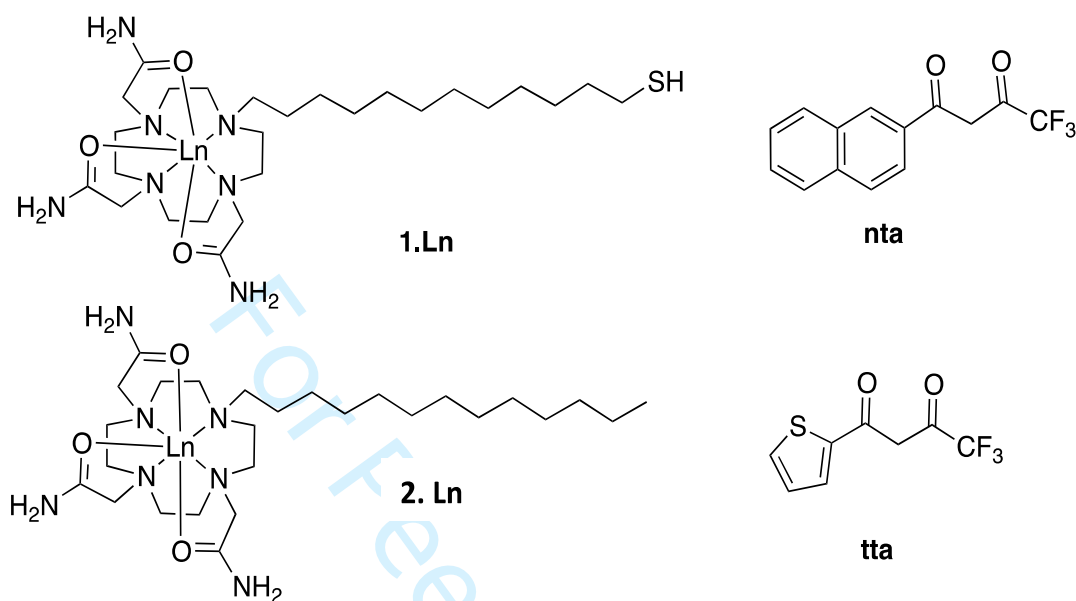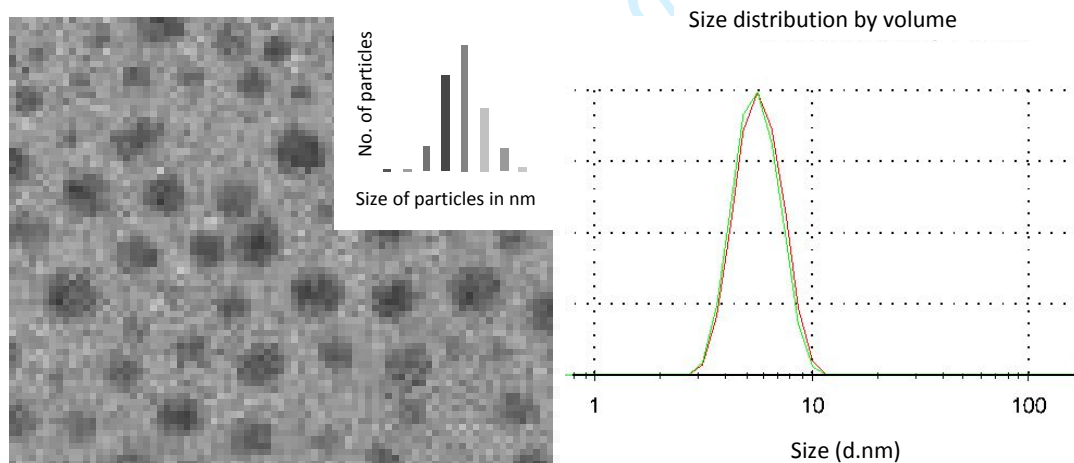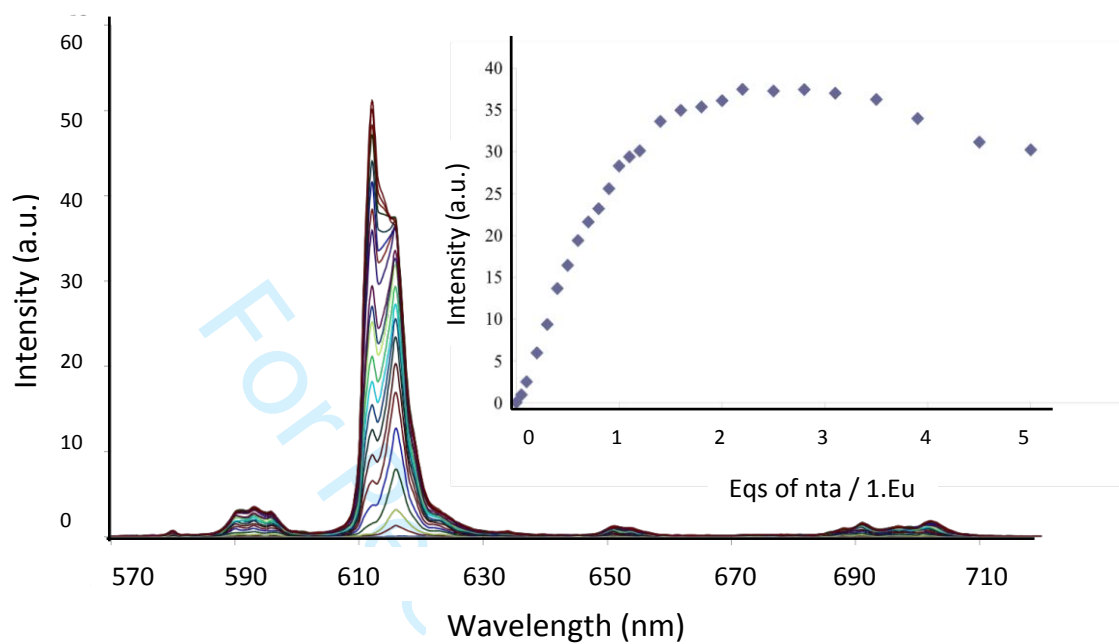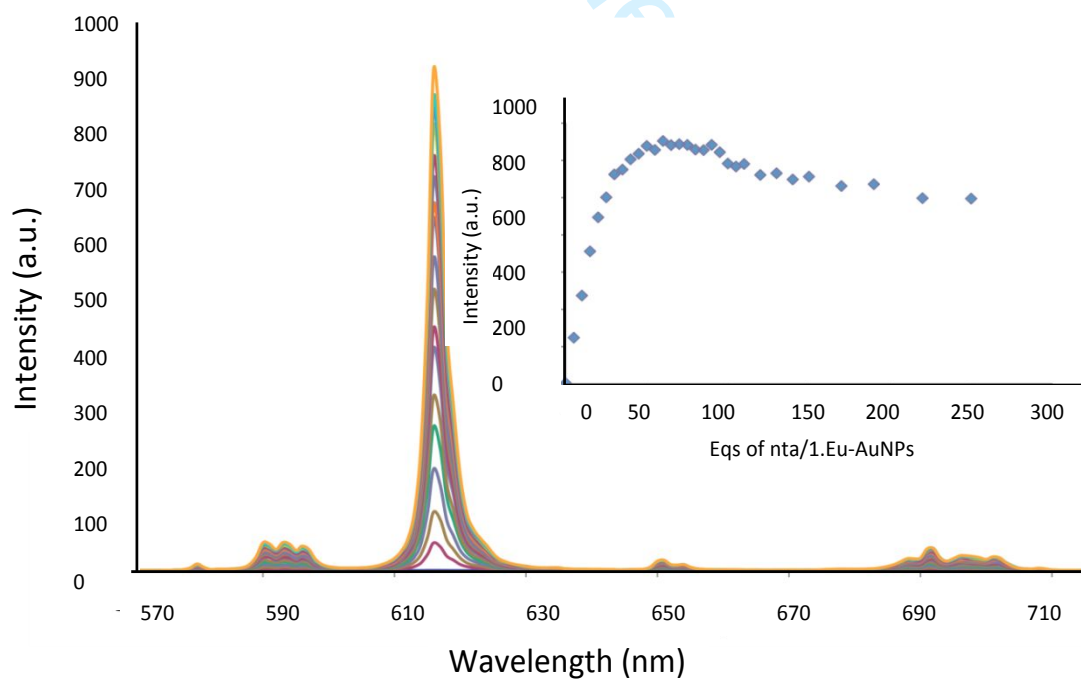
Figure 3

Figure 4

Figure 5
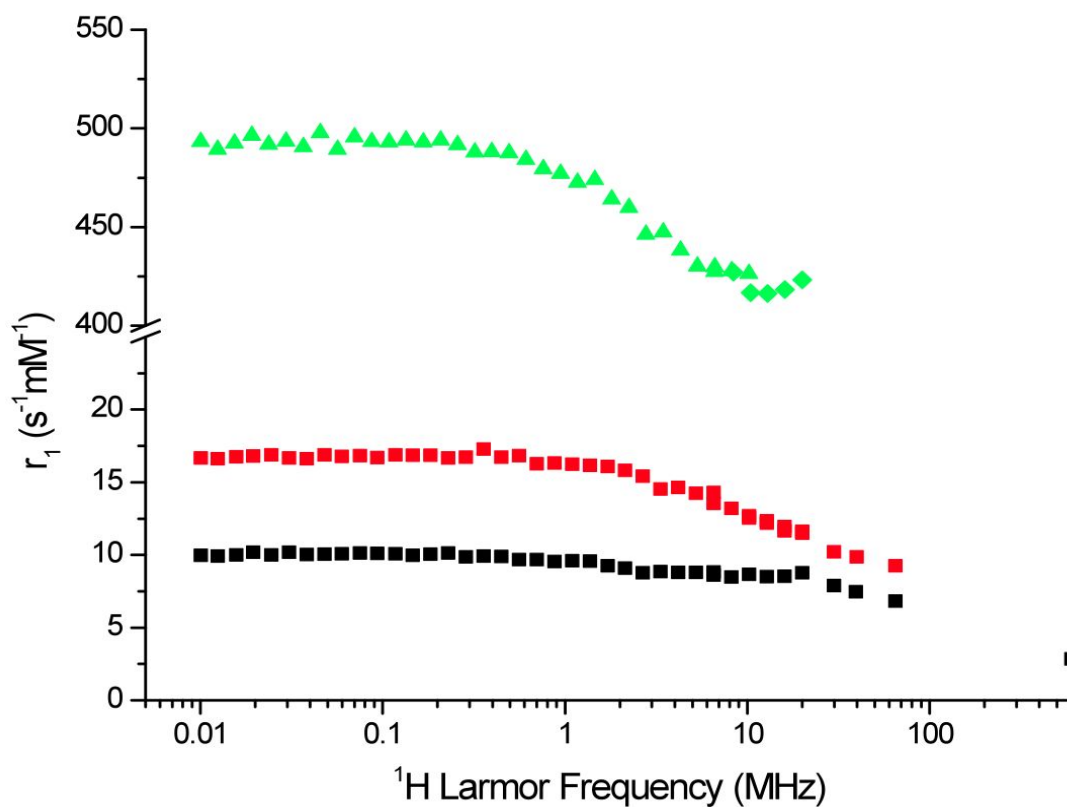
Table 1. Lifetime analysis of the L(III) complexes and conjugates. These were fully reproducable.

Complex	τ_{H2O} (ms)	τ_{D2O} (ms)	q value (± 0.5)
1.Eu	0.44	0.93	1.5
4. Eu	0.52	1.14	1.7
1.Tb	2.65	1.5	1.0
1.Eu-AuNPs	0.64	1.6	1.5
1.Tb –AuNPs	2.70	1.67	0.7

Ln(III) cyclen-based micelles and AuNPs conjugates as candidates for luminescent and magnetic resonance imaging (MRI) agents

Jennifer K. Molloy, Aline M. Nonat, John E. O'Brien, Dermot F. Broughamd and Thorfinnur Gunnlaugsson
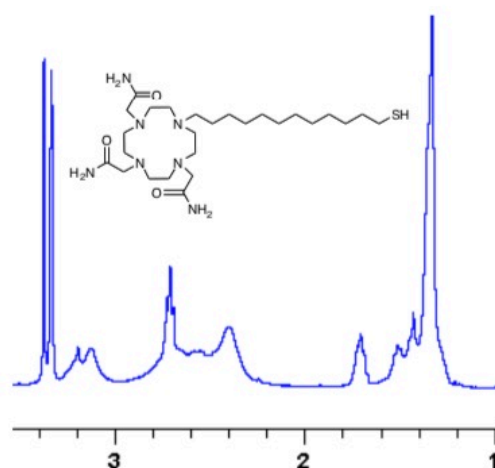
Figures

Figure S1: Partial ^{1}H NMR spectrum (MeOD, 400 MHz) of ligand **1**
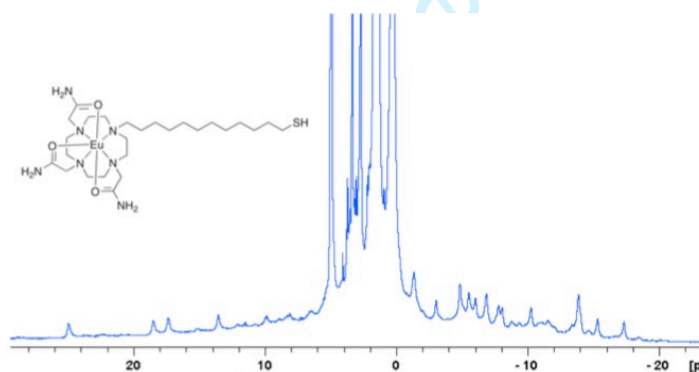
Figure S2: ^{1}H NMR spectrum (MeOD, 400 MHz) of **1.Eu**, showing the classical shifts in the axial and equatorial protons of the cyclen ring.
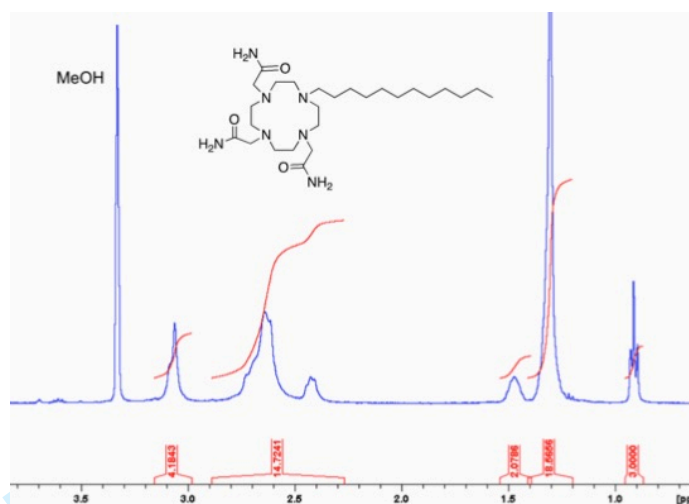
Figure S3: ^{1}H NMR spectrum (MeOD, 400 MHz) of ligand **2.**
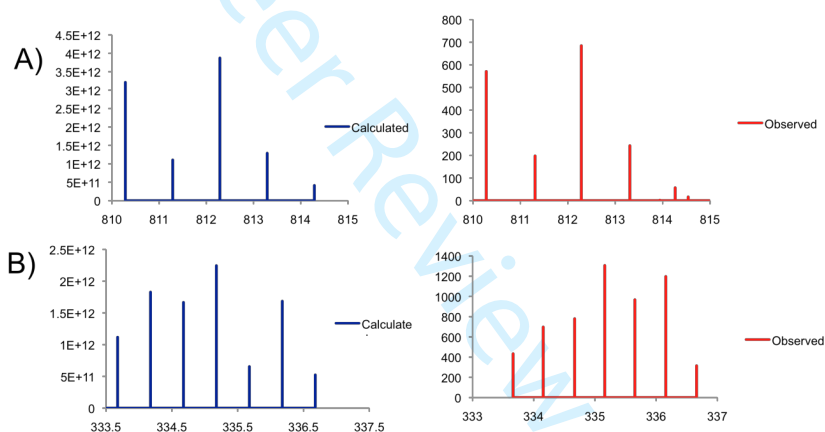
Figure S4: A) MALDI of **2.Eu** calculated and observed, **B**) MALDI of **2.Gd**, calculated and observed. The calculated and the observed isotopic distribution pattern of **2.Eu** and **2.Gd** obtained from the MALDI can be seen in Figure 1, which in the case of **2.Eu** was fitted to $C_{27}H_{52}N_7O_6F_3SEu$ with the calculated mass of 812.2864. Figure 1a, but similar results were observed for **2.Gd**, with an observed mass of 669.3474 for $C_{27}H_{52}N_7O_6F_3SGd$.
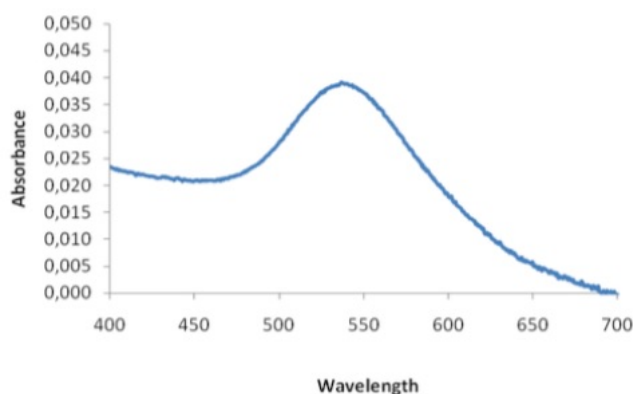
Figure S5: UV-Vis absorption spectrum of **1.Eu-AuNPs** in H_2O, showing the characteristic SPR band with λ_{max} at 520 nm. These particles were stable over time and no measurable change was observed after 6 months.
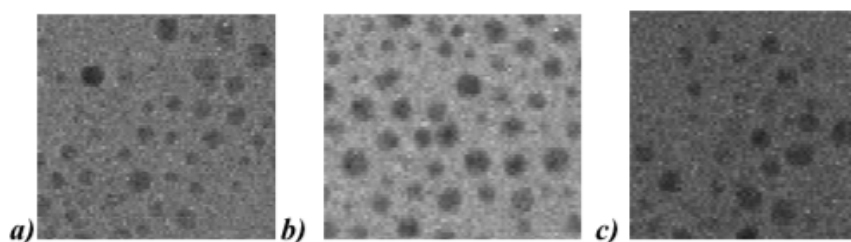
Figure S6: TEM images of **1.Ln-AuNP [Ln = a) Tb; b) Eu; c) Gd].** Characterisation of the nanoparticles by TEM, showed monodisperse stabilised particles.
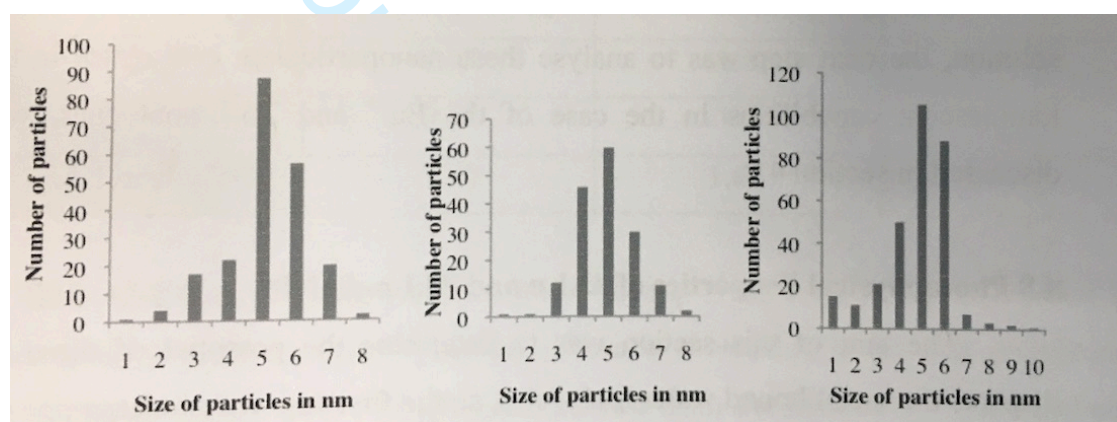
Figure S7: The size distribution of **1.Ln-AuNP [Ln =a) Tb; b) Eu; c) Gd]** determined from the TEM shown in Figure S6 above, was on average 5-6 nm, which are the size expected from the Brust method (Picture taken from the original analysis report).
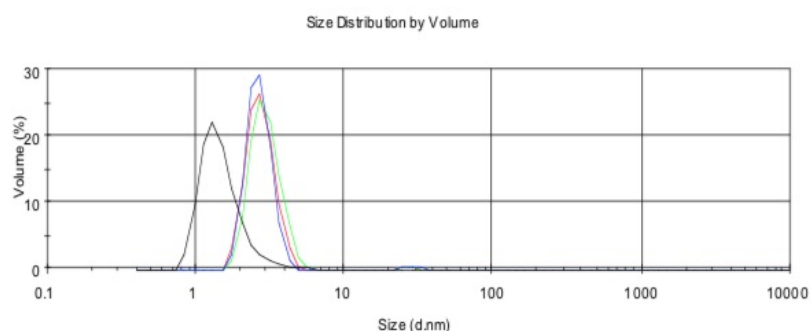
Figure S8: Hydrodynamic diameter (based on the value average particle size as measured by DLS) for **1.Ln-AuNP Ln = a) Tb (green); b) Eu (red); c) Gd (blue).**
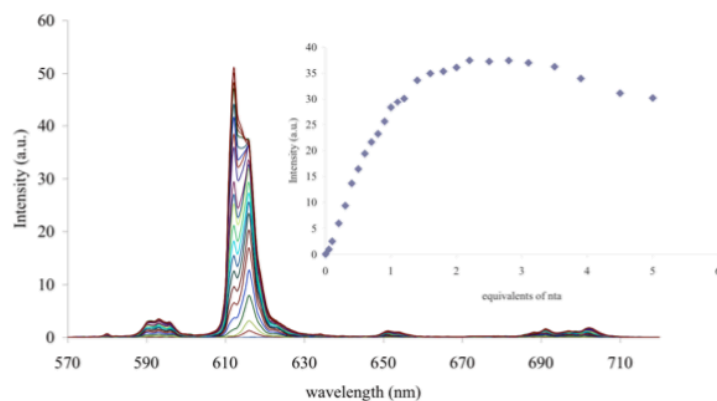
Figure S9: Changes in the Eu(III) (line-like emission bands at 580, 595, 616, 650, and 700 nm) phosphorescence spectrum upon titrating **1.Eu** (c =1 x 10- 5 M) with **nta** (0-6 equivalents). *Inset:* Experimental binding isotherm, for the emersing emission at 615 nm (the hypersensitive Δ J = 2 transition) versus equivalents of **nta.** This transition is particularly sensitive to the coordination environment of the Eu(III) centre, indicating the displacement of the metal bound water molecules and the formation of the complex with **nta.** The dramatic enhancement of red Eu(III) emission that was readily visible under a UV-lamp.
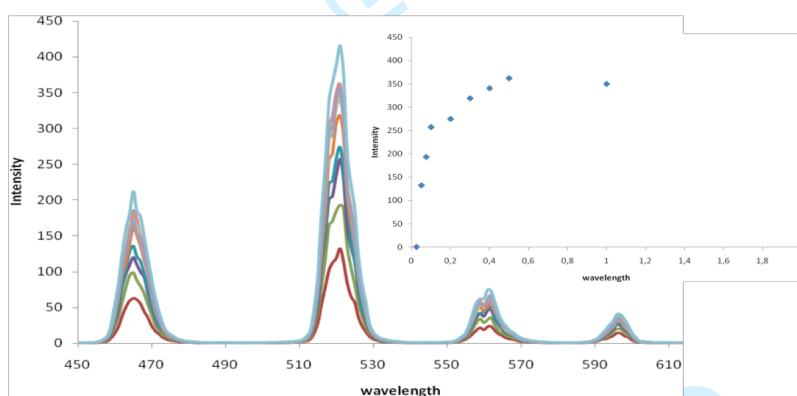
Figure S10: Changes in the Tb(III) phosphorescence spectrum upon titrating **1.Tb** (c=1 x 10⁻⁵M) with benzoic acid 0-6 equivalents. **Inset**: Experimental binding isotherm, emission intensity at 545 nm ($^5D_4$-$^7F_5$) versus equivalents of benzoic acid.
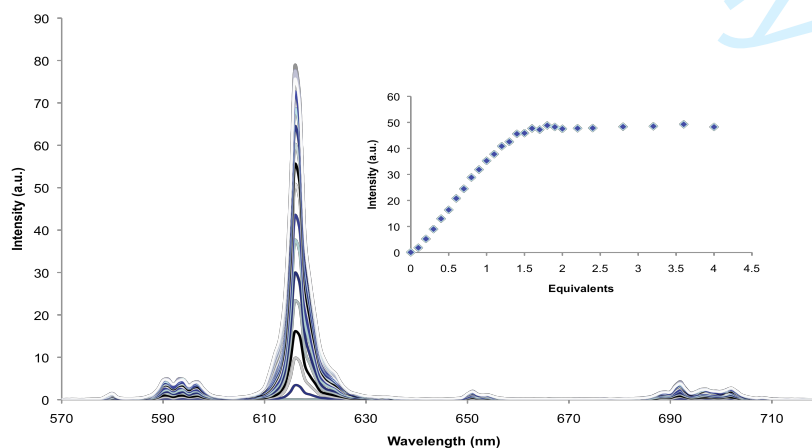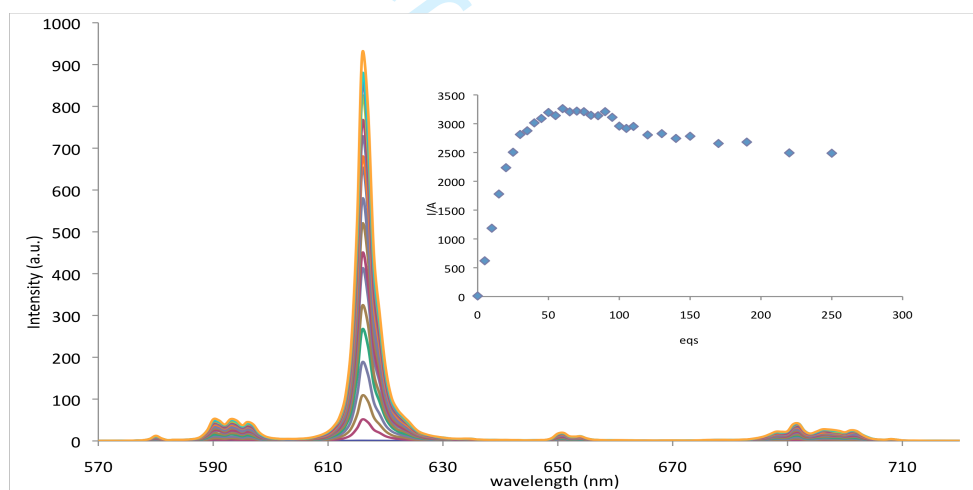

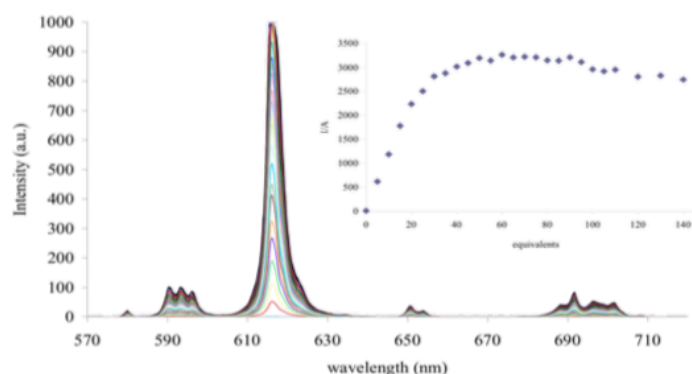**Figure S11:** The changes in the Eu(III) emission spectrum of **2.Eu** (c = 1 x 10-5) upon the

addition of **nta**. Inset: Experimental binding isotherm, emission intensity at 615 nm versus eqs of **nta**.
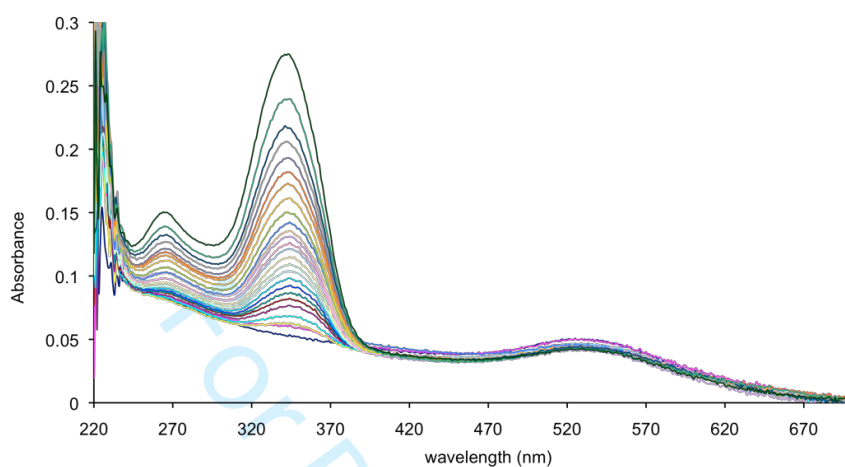
Figure S12: Evaluation of the UV-vis absorption spectrum of **1.Eu-AuNPs** (1×10^{-7}M) in HEPES buffered solution (0.1M, ionic strength 0.1M NaCl) upon addition of **tta** 0-250 equivalents.


Figure S13: The changes in the Ln^{3+} centred emission of **1.Eu-AuNPs** (1×10^{-7}M) in HEPES (0.1M, ionic strength 0.1M NaCl) upon the addition of **nta** 0-250 equivalents. **Inset:** The changes in the Eu^{3+} emission at 615 nm versus the number of equivalents of **nta** added.

Figure S14: Evaluation of the Eu^{3+} emission of **1.Eu-AuNPs** (1x10^{-7}M) in HEPES buffered solution (0.1M, ionic strength 0.1M NaCl) upon addition of **tta** 0-250 equivalents. **Inset:** shows the changes in the Eu^{3+} $^{5}D_{0}$-$^{7}F_{2}$ transition vs the number of equivalents added of **tta.**
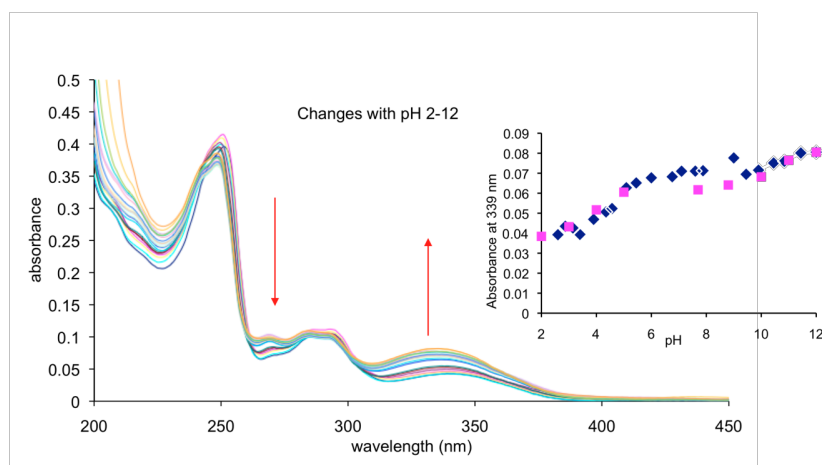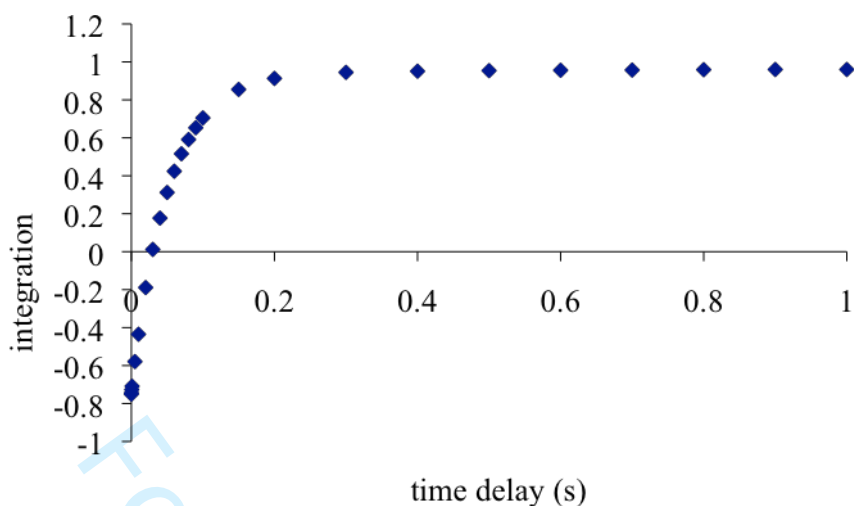

Figure S15: The changes in the UV-Vis absorption spectrum of **1.Eu-AuNPs-nta** as a function of pH 2-12. **Inset:** Changes in the UV-Vis absorption band at 339 nm as a function of pH with reverse titration overlaid.
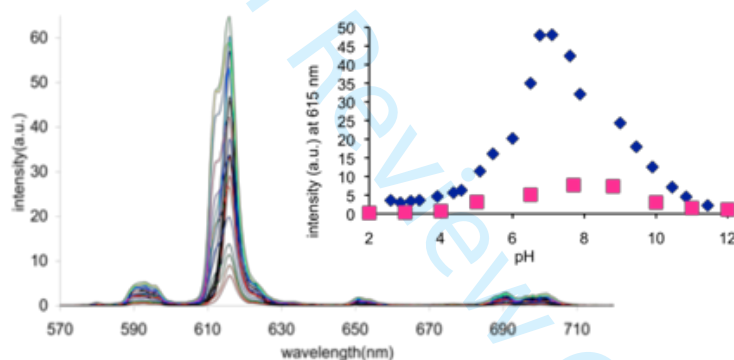
Figure S16: Evolution of the Eu^{3+} emission of **1.Eu-AuNPs-nta** with pH. **Inset**: Changes in the $^{7}F_{2}$ transition upon varying the pH from 2-12 (blue), reverse titration pH 12-2 (red).

a)

b)

*Longitudinal relaxivity r_1 for **1.Gd** complex*

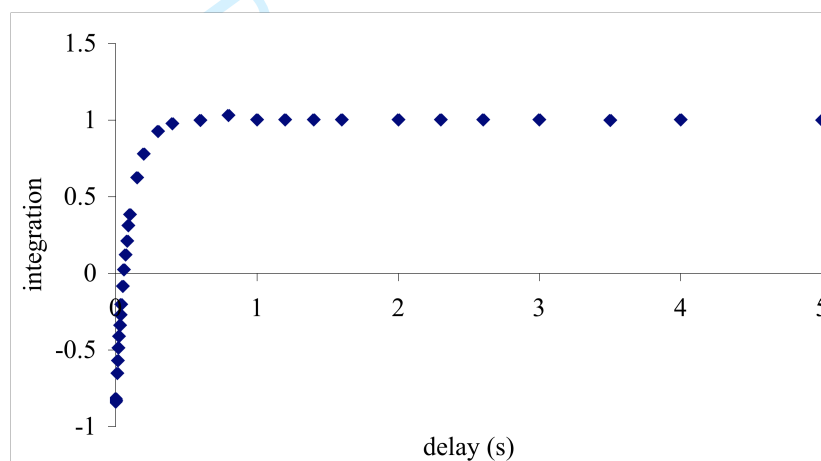| Frequency	10 MHz	400 MHz	600 MHz
r_1 [$s^{-1}mM^{-1}$]	16.5	11.14	8.1

Figure S17: **(a)** Plot of integration versus the time delay from ^{1}H NMR (400 MHz, D_2O) for the T_1 of **1.Gd** (2.67 mM). (**b**) From these measurements, the longitudinal water proton relaxivity r_1 (H_2O), which arises from **1.Gd** can be estimated by dividing the D_2O value reported in Table below by the viscosity ratio, h(D_2O)/h(H_2O) = 1.24. The longitudinal relaxation times of the H_2O protons in solutions of **1.Gd**, were also measured at 10 MHz and 298 K, using NMRD studies, and the corresponding relaxivities are reported in **b** and shown in the profile in **Figure S18**.
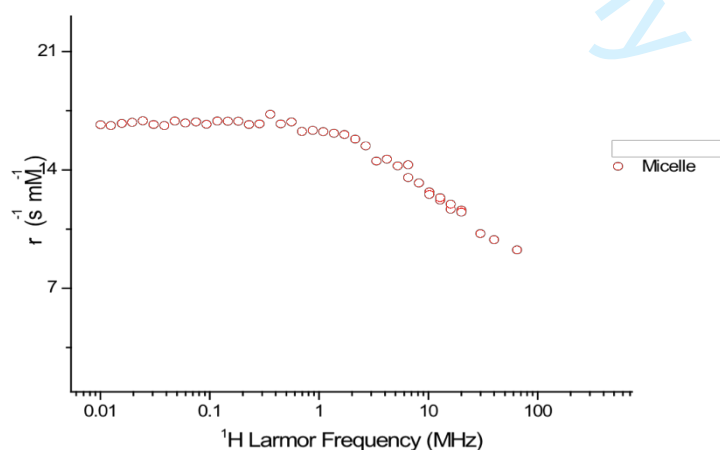
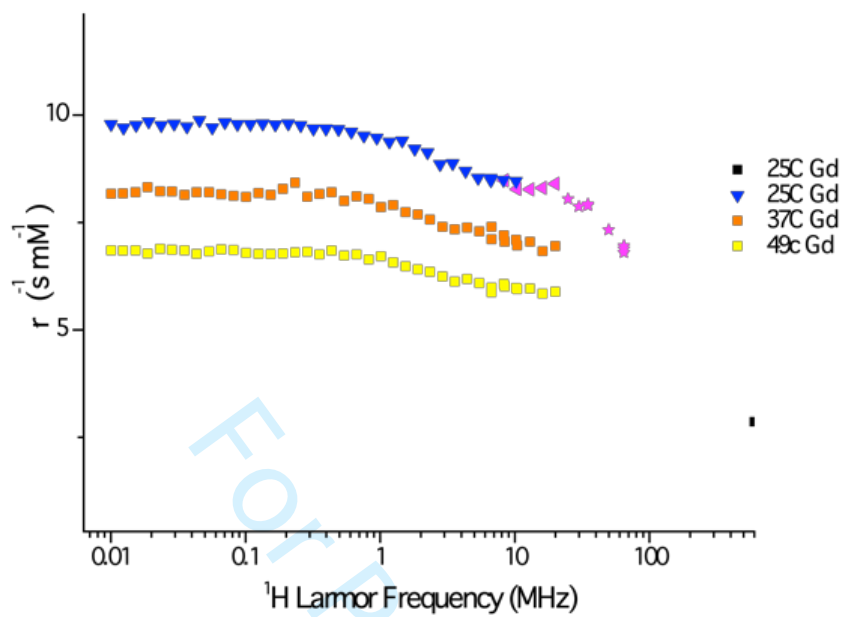**Figure S18**: Longitudinal relaxivity (r_1) of the H_2O protons of 1.**Gd** in H_2O at 298K (2.67 mM).
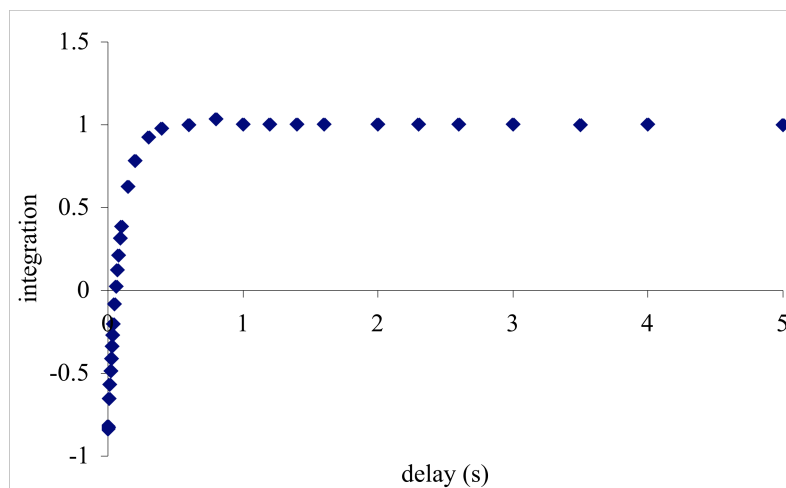
Figure S19: Plot of integration vs the delay of the values from ^{1}H NMR for the T_1 of **2.Gd**

Figure S20: Plot of integration versus the delay time for the T_1 of **1.Gd-AuNPs** in H_2O (2.67 mM)

Frequency MHz	10 MHz	600 MHz	400 MHz
r_1 [$s^{-1}mM^{-1}$] per Gd	16.5	8.1	11.14
r_1 [$s^{-1}mM^{-1}$] per AuNP	-	315	416.2

Figure S21: Relaxivity calculated **for 1.Gd-AuNPs**

1
2
3
4
5
6
7
8
9
10
11
12
13
14
15
16
17
18
19
20
21
22
23
24
25
26
27
28
29
30
31
32
33
34
35
36
37
38
39
40
41
42
43
44
45
46
47
48
49
50
51
52
53
54
55
56
57
58
59
60

Figure S22: Longitudinal relaxivity (r_1) of the protons of **1.Gd-AuNPs** in H_2O at 25 °C, 37 °C, 49 °C.